Forestry: An International Journal of Forest Research, 2026, 99(3), cpag028
https://doi.org/10.1093/forestry/cpag028
Published: 9 April 2026
Original Article

Institute of Chartered Foresters
OXFORD

Measuring forest inventory attributes using Faro Orbis Mobile laser scanner in managed boreal forests

Lauri Liikonen[1,*], Tuomas Yrttimaa[1,2], Aapo Erkkilä[1], Johanna Paakkari[1,3], Timo Pitkänen[4], Eetu Kotivuori[3], Mikko Vastaranta[1]

[1]School of Forest Sciences, University of Eastern Finland, P.O. Box 111, 80101 Joensuu, Finland
[2]Department of Forest Sciences, University of Helsinki, Latokartanonkaari 7, 00790 Helsinki, Finland
[3]Finnish Forest Centre, Siltakatu 20 B, 80100 Joensuu, Finland
[4]Natural Resources Institute Finland (Luke), Latokartanonkaari 9, Helsinki, 00790, Finland

*Corresponding author. School of Forest Sciences, University of Eastern Finland, Joensuu, North Karelia 80101, Finland. E-mail: laurliik@uef.fi

Abstract

Mobile laser scanning (MLS) provides detailed point cloud reconstructions of forest environments and has potential for operational forest sample-plot surveying. This study evaluated the accuracy of MLS in deriving forest inventory attributes, including basal area (G), number of trees per hectare (TPH), total stem volume (V), basal area-weighted mean tree diameter (Dg) and height (Hg), and dominant height (Hdom). Experiments were conducted in managed boreal forests across 44 sample plots (370–2000 m^2) using a Faro Orbis MLS system. Field measurements collected tree-by-tree (n = 4472) with callipers and clinometers during the previous summer served as reference data. We compared two alternative MLS data acquisition trajectories—closed loops (MLS-loop) and line transects (MLS-line)—and two processing workflows: (i) manually assisted tree detection followed by automatic tree measurements, and (ii) a fully automatic workflow. MLS-line provided similar or marginally improved accuracy compared with MLS-loop; however, the substantially shorter acquisition time of MLS-loop (19.0 min per plot on average) favoured its operational use over MLS-line (30.5 min). Clearer differences emerged between processing workflows. The fully automatic workflow identified and measured 74.1% of trees with diameter at breast height (DBH) > 5 cm, whereas manual assistance in tree detection increased this proportion to 97.1%. DBH accuracy was similar for both workflows (root-mean-square-error [RMSE] ≈ 2.4 cm), but tree-height estimates were substantially less accurate under automatic processing (RMSE 6.2 m) than under the assisted workflow (RMSE 2.1 m). These differences propagated to plot-level estimates. Using the automatic workflow, RMSEs were 4.2 m^2/ha for G, 610 trees/ha for TPH, 29.3 m^3/ha for V, 2.3 cm for Dg, 1.6 m for Hg, and 1.9 m for Hdom. The assisted workflow notably improved accuracy, yielding RMSEs of 3.5 m^2/ha for G, 54.0 trees/ha for TPH, 20.2 m^3/ha for V, 1.2 cm for Dg, 1.3 m for Hg, and 1.2 m for Hdom when using closed-loop trajectories. Overall, the results emphasize the importance of assisted workflows for attributes sensitive to detection completeness, particularly TPH, while showing that kinematic MLS can efficiently capture forest structure for sample plot measurements.

Keywords ground-based LiDAR, forestry, Faro Orbis, forest surveying

Introduction

Forest inventories—including national forest inventories (NFIs) based on statistical sampling as well as remote-sensing-based forest mapping—rely on measurements collected from sample plots (Tomppo *et al.* 2008). Within these plots, tree species and health status are typically identified, and diameter at breast height (DBH) and tree height are measured. Species identification and health assessment are generally based on the field surveyor's expertise, whereas DBH and height are obtained using callipers, measuring tapes, and clinometers. Stand age may also be determined by extracting increment cores from a subset of trees (Maltamo *et al.* 2021, White *et al.* 2025). Additional attributes commonly collected from sample plots include site fertility and deadwood characteristics, including downed woody debris (Russell *et al.* 2015). These tree-level measurements are subsequently used to derive plot-level forest inventory attributes such as number of trees per hectare (TPH), basal area (G), stem volume (V), dominant height (Hdom), and basal area-weighted mean diameter (Dg) and height (Hg) (Tomppo *et al.* 2008, Maltamo *et al.* 2021, White *et al.* 2025). Precise georeferencing of sample plots is also required to link field observations with remotely sensed data for large-area estimation (e.g. Gobakken and Næsset 2009). Tree-level forest inventories derived from remote sensing further require knowledge of the spatial locations of individual trees within plots to enable matching between field observations and

Handling editor: Dr. Lars Waser
Received: 2 July 2025. **Revised:** 20 January 2026. **Accepted:** 8 March 2026

remote-sensing-derived tree-level metrics (Maltamo *et al.* 2014). Plot sizes may vary from a few tens of square metres in young-stand inventories to nearly one hectare in inventories supporting satellite-based interpretation (e.g. Wilkes *et al.* 2017). The number and size of sample plots required depend on the purpose of the inventory and are often constrained by available resources and measurement technologies.

Despite advances in remote-sensing technologies, the collection of tree- and stand-level attributes from field sample plots—and the accurate geolocation of these plots—remains a fundamental and challenging task. Navigation to plots typically relies on a Global Navigation Satellite System (GNSS) receiver, and measuring the spatial locations of individual trees often requires additional positioning instruments or methods (Kostensalo *et al.* 2023, Liu *et al.* 2025). Tree-height measurements with a clinometer are sufficiently labour-intensive that heights are usually measured only for a subset of trees (Eerikäinen 2009). Likewise, stem-quality attributes—such as branching characteristics, taper, or defects—are typically not measured, or cannot be measured with sufficient accuracy to justify carrying additional equipment such as upper-stem diameter gauges. Mapping of downed deadwood is similarly time-consuming and is frequently omitted unless specifically required. Owing to the range of equipment needed and the overall workload involved, sample plots are often measured by two field personnel, further increasing the cost of data collection.

Efforts to improve sample plot measurements have increasingly focused on laser scanning and imaging techniques (Morsdorf *et al.* 2018, Iglhaut *et al.* 2019). These techniques have been applied using static instruments within the forest (e.g. Dassot *et al.* 2011), by moving through the stand (Bauwens *et al.* 2016), or with drones capturing data both above and within the canopy (Jaakkola *et al.* 2010, Westoby *et al.* 2012, Chisholm *et al.* 2013). Such approaches produce detailed point-cloud reconstructions of trees within sample plots, enabling the determination of trees' spatial positions (Simonse *et al.* 2003, Aschoff and Spiecker 2004), the measurement of stem dimensions at multiple heights (Liang *et al.* 2014a, Olofsson and Holmgren 2016), and the characterisation of tree crown structures (Henning and Radtke 2006). They also offer the potential for simultaneous mapping of downed deadwood together with standing trees (Yrttimaa *et al.* 2019). The level of instrumentation required may be sufficiently reduced to allow data collection by a single operator (Holvoet *et al.* 2025). However, measurements acquired from above the canopy have not yet reached the accuracy required for sample-plot inventories (Hyyppä *et al.* 2020), and below-canopy measurements therefore remain necessary. Consequently, considerable effort has focused on terrestrial and mobile laser scanning (TLS and MLS) to automate or streamline forest sample-plot measurements. TLS provides high geometric accuracy and produces detailed three-dimensional point-cloud data (Dassot *et al.* 2011), enabling accurate estimation of tree height, DBH, and other attributes (e.g. Holvoet *et al.* 2025). However, important challenges in ground-based lidar remain. First, not all trees can necessarily be detected from the collected data, particularly small or occluded trees are still often missed (Liang *et al.* 2018). Second, tree species classification derived from these methods has not yet reached the reliability of field-based assessments by experienced surveyors (Puliti *et al.* 2025). Third, the derivation of tree- and stand-level attributes from the collected 3D point clouds is still not fully automated, and readily available software solutions remain limited (Murtiyoso *et al.* 2024). In addition, TLS-based inventories typically require multiple scan positions and subsequent point-cloud registration (Liang *et al.* 2016), which increases field time. Despite improvements in portability and scanning speed (e.g. Verhelst *et al.* 2024), plot-level TLS data acquisition remains time-consuming, motivating interest in more mobile alternatives.

MLS largely overcomes the mobility constraints and vegetation-induced occlusion issues associated with TLS (Liang *et al.* 2022). MLS devices collect point-cloud data while the operator is in motion, enabling substantially faster data acquisition. This efficiency gain, however, is accompanied by somewhat reduced geometric accuracy and precision (Liang *et al.* 2014b, Hunčaga *et al.* 2020). An MLS system typically comprises a laser scanner, a GNSS positioning unit, and an inertial measurement unit (IMU) that records device orientation. Even high-grade GNSS–IMU systems can exhibit positioning errors on the order of tens of centimetres in forested terrain, where canopy cover attenuates and reflects GNSS signals (Kukko *et al.* 2017). These limitations can be mitigated using Simultaneous Localization and Mapping (SLAM) algorithms, which co-register point-cloud data by detecting objects repeatedly scanned during acquisition, thereby compensating for GNSS- and IMU-related errors (Kukko *et al.* 2017, Gollob *et al.* 2020). MLS benefits substantially from SLAM, and recent advancements (e.g. Wu *et al.* 2025) further enhance MLS's potential as a practical tool for modern forestry (Holvoet *et al.* 2025).

Numerous studies have examined the performance of MLS in deriving forest inventory attributes (Balenović *et al.* 2021). Hrdina *et al.* (2025) compared several automatic tree detection and measurement algorithms with an assisted approach in a two-storey forest stand comprising 236 trees. The manual point-cloud measurements achieved a tree detection rate of 99.2% with a DBH root-mean-square-error (RMSE) of 1.2 cm, whereas the fully automatic 3DFin algorithm reached 77.1% detection with a DBH RMSE of 2.4 cm. These results are consistent with typical MLS measurement accuracies reported in the literature (Gollob *et al.* 2020, Kükenbrink *et al.* 2025, Sofia *et al.* 2024). Despite advances in MLS sensor technology and improvements in computational solutions, MLS performance under operational forest-survey conditions—where sample plots across diverse forest structures are measured tree by tree—remains insufficiently documented. Likewise, the influence of MLS data acquisition strategies and processing workflows on the accuracy of sample-plot measurements is still largely unknown.

The aim of this study was to address this knowledge gap by evaluating the feasibility of MLS for surveying boreal forest sample plots within an operational inventory setting. We used sample plots selected to represent the structural variability required for producing accurate ALS-based forest resource information across an entire inventory region. Using calliper- and clinometer-based field measurements as reference data, we assessed the accuracy of MLS in detecting individual trees and measuring their dimensions for estimating key forest inventory attributes: TPH, G, V, Hdom, Dg, and Hg. To evaluate the operational feasibility of MLS technology, we compared performance differences (i) between two MLS data acquisition trajectory designs and (ii) between two different data processing workflows, one incorporating manual assistance ('assisted workflow') in tree detection and the other relying on a fully automatic procedure ('automatic workflow').

Materials and methods

Experimental design

The study area was located in Heinävesi, Eastern Finland (62.37°N, 29.00°E; Fig. 1) covering 264 600 ha. It represents typical eastern

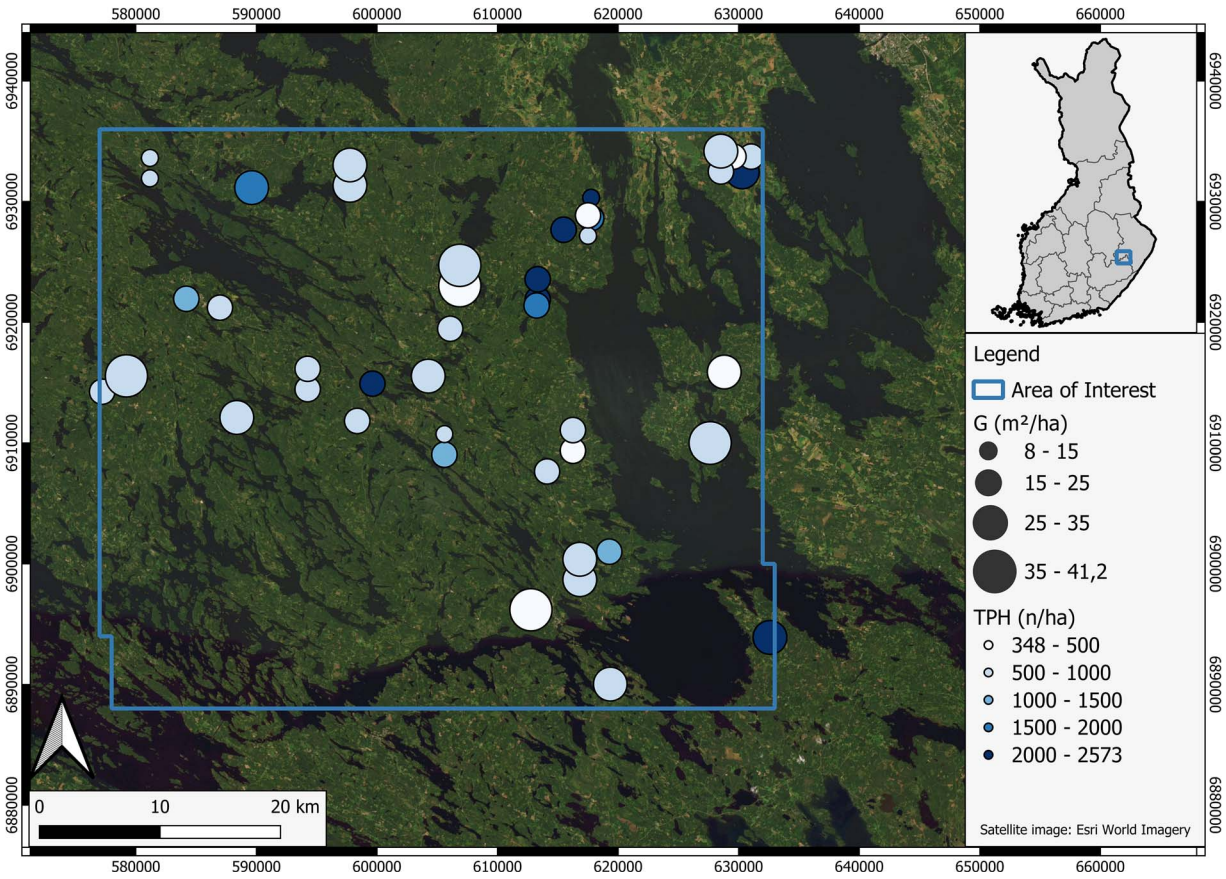

Figure 1 Map of the study area located in Heinävesi, Finland, on top of a satellite imagery with circles showing the locations of the sample plots, the circle size and colouring indicating variation in basal area (G) and the number of trees per hectare (TPH), respectively.

Finnish forest conditions, consisting predominantly of privately owned managed stands. The dominant tree species are Scots pine (*Pinus sylvestris L.*), Norway spruce (*Picea abies (L.) Karst.*), and birches (*Betula spp.*). The study area is one of the operational inventory regions of the Finnish Forest Centre. From all such regions, forest inventory attributes are mapped for forest planning purposes by acquiring an area-wide ALS dataset and establishing sample plots to collect field information on forest attributes.

In summer 2023, the Finnish Forest Centre established and measured 926 sample plots across the study area. From these, a representative subsample of 48 sample plots was selected. The selection aimed to preserve structural variability within the subsample by using Hdom, G, and dominant tree species as the selection criteria, ensuring that the sample represented the diversity of forest stands within the inventory area. The sample plot size was not fixed, as the Finnish Forest Centre aims to measure ~100 to 200 trees per plot to balance sampling accuracy with operational feasibility. Plot boundaries were delineated manually using ALS-derived canopy height model (CHM), with the boundaries aligned to tree crown edges. As a result, plot sizes ranged from 370 to 2015 m^2, with an average of 1152 m^2 (Table 1). In total, the reference plots contained 4472 trees, with plot-level number of trees varying between 40 and 227 (Fig. 2).

Reference measurements

The reference measurements were collected following the Finnish Forest Centre's sample plot measurement guidelines for ALS-based operational stand-level forest inventories. Tree species were recorded and DBH measured for all trees with DBH exceeding 5 cm using automatic data-logging callipers. Trees were also visually inspected and tagged if dead, bent, or broken. Approximately every fifth tree was selected as a sample tree, for which height was measured using an electronic clinometer. These sample trees were used to calibrate plot-level species-specific height models, allowing height prediction for non-sample trees based on their measured DBH (Eerikäinen 2009).

A tree map was generated using a TerraHärp pseudolite-based positioning system integrated with Masser ExCaliper II calipers, enabling the recording of tree positions in a plot-local coordinate system during DBH measurements (Kostensalo *et al.* 2023). Using GNSS measurements from ground control points located at plot corners, the tree map coordinates were transformed into the global ETRS-TM35FIN coordinate system.

Single tree stem volume was estimated using species-specific volume equations with DBH and height as explanatory variables (Laasasenaho 1982). Plot-level forest inventory attributes were then derived by aggregating the tree-level measurements for each sample plot. The variability in these attributes across the sample plots is summarized in Table 1.

Mobile laser scanning data acquisition

MLS data were acquired using a Faro Orbis scanner mounted on a backpack rack and operated in kinematic mode, allowing continuous point cloud data recording while moving (Fig. 3). The scanner has

Table 1 Descriptive statistics of reference tree attributes (H = tree height, DBH = diameter at the breast height) and forest inventory attributes (G = basal area, TPH = number of trees per hectare, dg = basal area-weighted mean diameter, Hg = basal area-weighted mean height) and sample plot area.

Attribute	Mean	Min	Max	STD
H (m)	15.8	1.4	36.6	7.2
DBH (cm)	16.5	5.1	53.0	8.8
Hg (m)	19.9	8.2	29.0	5.8
Dg (cm)	22.5	9.4	35.5	7.4
G (m^2/ha)	23.4	8.0	41.2	8.1
V (m^3/ha	233.0	62.2	495.4	125.4
TPH (n/ha)	1021	348	2573	640
Area (m^2)	1152	370	2016	410

The statistics are based on a subset of 44 sample plots for which mobile laser scanning (MLS) data were successfully acquired.

Figure 2 Photographs of example sample plots demonstrating the structural variability among the sample plots. TPH = number of trees per hectare (n/ha), Hg = basal area-weighted mean height (m), Dg = basal area-weighted mean diameter (cm), G = basal area (m^2/ha), V = stem volume (m^3/ha) based on reference measurements.

a maximum range of 120 m and a 360° × 290° field of view, with 32 laser channels (wavelength of 905 nm) and a scanning speed of 640 kHz, achieving an accuracy of 5 mm (1σ). The system weighs 3.60 kg (2.10 kg for the scanner and 0.95 kg for the data logger) and provides ∼3 hours of continuous battery life. For georeferencing, the Faro Orbis was paired with a Trimble DA2 GNSS receiver connected to a virtual reference station (VRS) provided by Trimnet and operated through the Penmap mobile application. Under favourable conditions, this setup provided decimetre-level localisation accuracy.

The MLS data acquisition was conducted between late May 2024 and early September 2024 using two different data acquisition trajectory patterns. The first pattern was a line-transect trajectory (hereafter referred to as 'MLS-line'), in which the operator walked along crossing transect lines (Fig. 4). The second pattern consisted of four closed loops that intersected at the plot centre (hereafter referred to as 'MLS-loop'). Trajectory planning accounted for the requirements of the 3D SLAM methodology used by the Faro Orbis system. SLAM operation relies on the 'close-the-loop' principle, meaning that the trajectory should start and end at the same location to minimize drift (Di Stefano *et al.* 2021). The 3D SLAM algorithm processes raw laser-scanned data into a point cloud by repeatedly detecting stable features in the environment, such as tree stems. For a feature to be reliably recognized, its size-to-range ratio should be ∼1:10; for example, a tree with a 20 cm diameter becomes a significant feature when scanned at distances shorter than

Figure 3 Illustration of the mobile laser scanning setup including a Faro Orbis scanner paired with a Trimble DA2 GNSS receiver.

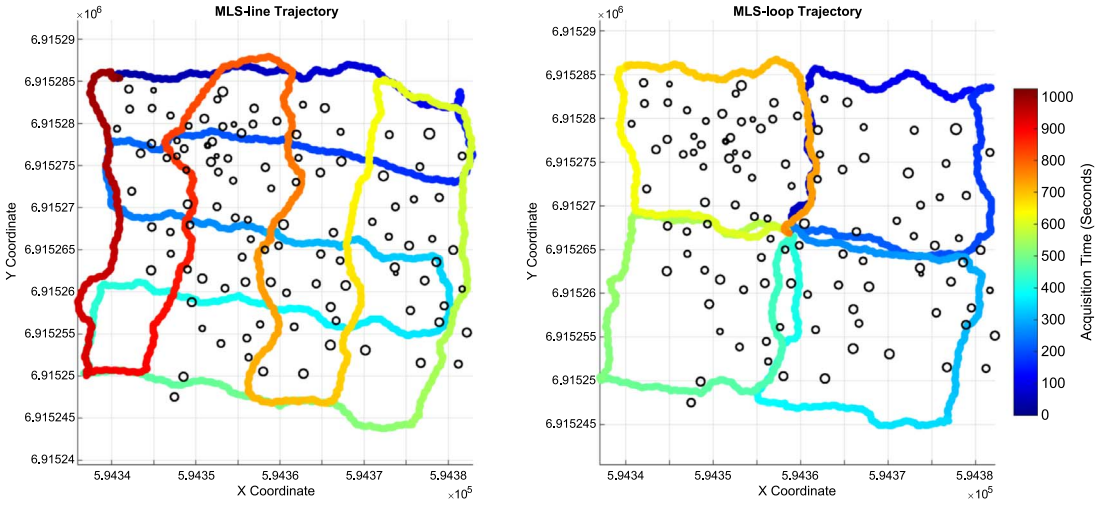

Figure 4 Illustration of the two mobile laser scanning (MLS) data acquisition trajectories used in this study: Line-transect trajectories ('MLS-line,' left) and closed-loop trajectories ('MLS-loop,' right) on a 37 m × 37 m sample plot. Colours indicate acquisition time. Black circles show tree locations based on reference measurements.

2 m. Frequent loop closures are recommended because they distribute accumulated error across the trajectory. The scanner manufacturer therefore advises using circular loops instead of retracing steps (FARO 2024).

The MLS trajectories were designed so that, in the MLS-line approach, the line transects intersected at intervals of ∼10 m for plots with a TPH < 1000 n/ha and at ∼5 m for plots with a TPH ≥ 1000 n/ha. For MLS-loop, the spacing between adjacent trajectory segments was roughly twice that of MLS-line (Fig. 4).

The scanner was operated using the Faro Sphere mobile application, which displayed the real-time walking trajectory to support data acquisition. Using the Faro Sphere application, reference points were recorded at each plot corner and at the plot centre. These reference points were subsequently linked to the control points captured with the Penmap application. A rigid coordinate transformation—including XY translation and Z-axis rotation—was then applied in the Faro Connect (version 2024.2) software to align the MLS-derived point cloud with the global coordinate system.

Because the number of recorded points depends on acquisition time, walking speed was kept as consistent as practical under field conditions. After closing the loop and ending the trajectory, the SLAM algorithm required a finalisation period during which scanning was disabled. The final SLAM processing was performed in the Faro Connect desktop software, where the point cloud was georeferenced and exported as a.*laz* file. Out of the 48 sample plots initially measured, four were discarded because data capture failed for one of the two trajectory designs, leaving 44 plots for analysis.

Assisted workflow for processing MLS data into forest inventory attributes

Point cloud data pre-processing

In the assisted workflow, the detection and segmentation of individual trees (instance segmentation) were performed in RiSCAN PRO (version 2.20.1; Riegl Laser Measurement Systems GmbH, Horn, Austria) using the LIS TreeAnalyzer plugin developed by Laserdata GmbH (Innsbruck, Austria) (Groiss and Handl 2024). The plugin is designed for processing data recorded by the Riegl scanners and therefore requires specific point attributes: XYZ coordinates, distance-corrected intensity (*Reflectance*), and a measure of pulse-shape deviation (*Deviation*).

Because our data did not originally include *Reflectance* or *Deviation*, these attributes were derived from the raw point cloud (Fig. 5, stage 1). *Reflectance* was created by linearly rescaling the original intensity values to the required range of −25 dB to 10 dB and removing extreme outliers as noise. *Deviation*, which tends to be low for planar stem surfaces and higher in heterogeneous neighbourhoods such as foliage (Yrttimaa *et al.* 2025), was estimated from local point-cloud geometry. For each point, surface normals were computed within a 3 cm neighbourhood, their orientations were stabilized using a Minimum Spanning Tree algorithm with six neighbours, and the absolute Z-components were extracted and rescaled to the 1–21 range expected by LIS TreeAnalyzer. All pre-processing steps were performed in CloudCompare (version 2.13.2).

The prepared point cloud was imported into RiSCAN PRO, where ground points were classified using standard procedures (Axelsson 2000). This classification enabled the creation of a digital elevation model and subsequent normalisation of Z-coordinates to represent height above ground level, required for tree-level characterisation with the LIS TreeAnalyzer extension.

Manually verified tree detection and instance segmentation

The LIS TreeAnalyzer identifies individual trees from a horizontal slice of the point cloud—typically extracted between 1.3 and 2.5 m above ground—with a thickness of 0.1–0.5 m. In this slice, tree cross-sections generally appear as circular or arc-shaped clusters, enabling their detection through point-cloud clustering and pattern-recognition techniques (e.g. Aschoff and Spiecker 2004). To suppress branch-related noise and improve the robustness of the tree detection process, a temporary filtering step was applied to remove points with Reflectance ≤10 dB and Deviation >3.

The remaining points—representing potential tree stem cross-sections—were projected onto the XY plane (Fig. 5, stage 2). A Hough Circle Transform (Illingworth and Kittler 1987) was then applied to detect circular features corresponding to tree stems. Manual verification was subsequently conducted to remove false detections caused by branches or understory vegetation forming arc-shaped

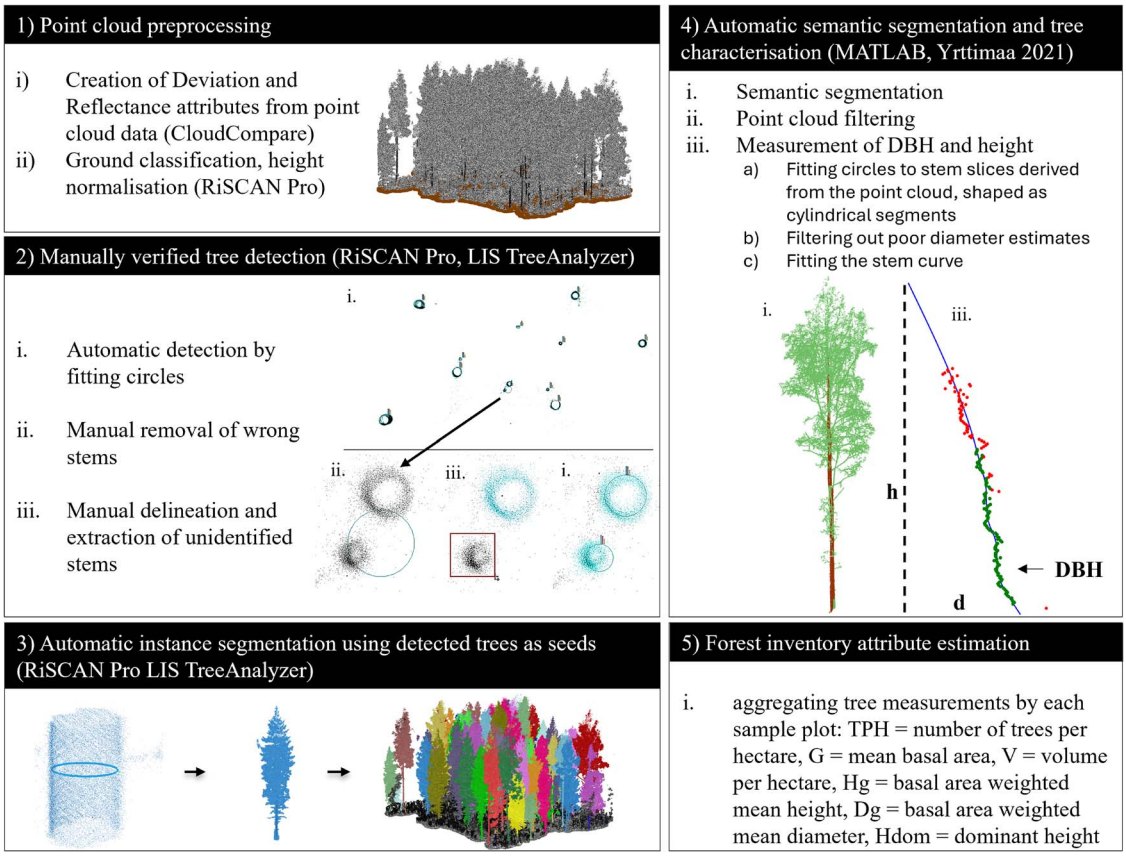

Figure 5 Overview of the *assisted workflow* for processing mobile laser scanning (MLS) data into forest inventory attributes**.** (1) Point cloud preprocessing: (i) Extraction of deviation and reflectance attributes, followed by (ii) ground classification and point cloud normalisation. (2) Manually verified tree detection: (i) Automatic detection through automatic circle fitting, (ii) manual removal of incorrect stems, and (iii) manual delineation of unidentified stems. (3) Automatic instance segmentation using detected trees as seeds. (4) Automatic semantic segmentation and tree characterisation using point cloud tools (Yrttimaa 2021). Diameters were measured by fitting circles to stem slices derived from cylindrical point cloud segments (iiia), omitting outliers (iiib), and fitting cubic splines as stem curves (iiic) to extract tree attributes, including DBH and tree height (h). (5) Forest inventory attributes were then estimated by aggregating tree-level metrics to forest inventory attributes such as basal area (G), number of trees per hectare (TPH), total stem volume (V), basal area-weighted mean tree diameter (Dg) and -height (Hg), and dominant height (Hdom).

patterns. Simultaneously, stem clusters missed by the automatic circle detection were manually delineated to ensure that all trees recorded in the point cloud became correctly detected.

The verified tree positions were then used as seeds for an automatic bottom-up segmentation approach that delineated entire trees—including stems and branches—within the point cloud (Fig. 5, stage 3). Following Bremer *et al.* (2018), a 3D Dijkstra Region Growing algorithm was applied, computing the shortest paths from each seed point towards the canopy top and grouping points based on their lowest-cost paths. Gaps of 0.15–0.6 m were tolerated during this process. Once points were labelled by tree instance, the segmented tree point clouds were exported with additional attributes, including tree location, tree height (defined as the maximum Z-value within each segment), and the diameter of the circle fitted to the stem cross-section.

Because the VRS-aided GNSS positioning did not always achieve the desired accuracy, the segmented tree point clouds and detected tree locations were georeferenced to the field-measured tree positions. A rigid coordinate transformation was computed by identifying corresponding trees (n = 5–10 per plot) in both datasets to serve as tie points. This ensured that MLS-derived measurements could be reliably linked to the corresponding reference measurements for subsequent accuracy assessment.

Semantic segmentation and tree- and forest inventory attribute estimation

The Tree attribute measurements were derived using the automated methodology originally introduced by Yrttimaa *et al.* (2019, 2020). This approach utilizes semantic segmentation to separate stem points from foliage and branches, thereby isolating the stem surface for taper curve estimation and subsequent attribute retrieval (Fig. 5, stage 4). The methods were implemented in MATLAB (The Mathworks Inc., Natick, MA, USA) and are openly available (Yrttimaa 2021). As these tools were initially designed for TLS data, additional point cloud filtration steps and parameter adjustments were necessary to ensure compatibility with the MLS data. These adjustments primarily involved relaxing tolerances to allow more scattered surface representations to be accepted as potential stem points, accounting for the inherent noise in MLS point clouds.

The segmentation process began by analysing local point neighbourhoods to identify smooth, vertical surfaces. These candidates were validated using a RANSAC-based cylinder filter (Fischler and Bolles 1981, Yrttimaa *et al.* 2020). Stem-crown separation was further refined through a Cartesian-to-cylindrical coordinate transformation and a Simple Morphological Filter (Yrttimaa *et al.* 2024). To effectively manage noise—particularly in the less dense upper sections of the

canopy—the DBSCAN algorithm (Ester *et al.* 1996) was applied to stem points across three distinct height intervals (0% . . . 30%, 30% . . . 70%, and 70% . . . 100%.). Finally, to prevent diameter overestimation, the stem points underwent a secondary Simple Morphological Filter pass similar to that used during the initial surface classification.

For the construction of taper curves, least-squares circles were fitted to 5 cm thick slices at 3 cm vertical intervals. To ensure accuracy, erroneous diameter measurements resulting from misclassified points or incomplete reconstruction were detected and removed using a second-order polynomial RANSAC fit and an adaptive window filter. Estimates were accepted only if they deviated by less than 5% from the mean of the five preceding measurements. A monotonic cubic spline (smoothing parameter 0.6) was subsequently fitted to interpolate missing sections (e.g. treetops) and smooth irregularities. The final DBH was derived directly from this taper curve.

To maximize the number of successfully measured trees despite variations in shape, size, and point cloud quality, a three-stage iterative procedure was employed. The first stage applied the strictest criteria regarding slice properties, outlier removal thresholds, and the minimum number of acceptable diameter measurements (at least nine). Trees failing these criteria were passed to a second stage, which allowed for greater uncertainty in circle fitting and densified the measurement interval along the stem from 3 cm to 1 mm. If necessary, a third stage further relaxed consistency requirements to accept trees with a minimum of six valid diameter measurements. This stepwise approach balanced measurement reliability with dataset completeness, minimising accuracy losses while maximising the extraction of tree-level attributes.

For trees where a full taper curve could not be successfully reconstructed, a fallback procedure was applied. This involved estimating DBH by repeatedly fitting a RANSAC-based cylinder model (200 iterations) to a 1-m thick stem section located between 1 m and 2 m above ground. Tree height was defined as the vertical difference between the lowest and highest points in the segmented cluster. As the complete stem taper curve was not available for all the measured trees, stem volume was predicted using the species-specific volume equations (Laasasenaho 1982) that were also used with respective reference measurements. For this task, the dominant tree species—identified from panoramic images captured within each plot—was assigned to all individual trees located within the corresponding plots.

After deriving the tree attributes, trees exhibiting unrealistic height–diameter ratios—indicating potential errors in either height or diameter—were identified as outliers and excluded from further analysis. This was done by fitting a logarithmic model to the height–diameter observations and comparing the predicted ratios with the measured ones. Outliers were detected using the two-sigma rule, assuming that 95% of the measurements should fall within two standard deviations of the mean. As a result, 116 trees detected from the MLS-line data and 113 trees from the MLS-loop data were removed as outliers. Tree measurements passing this procedure were subsequently aggregated at the plot level to derive estimates for TPH, G, V, Dg, Hg, and Hdom (Fig. 5, stage 5).

Automatic workflow for processing MLS data into forest inventory attributes

For processing the MLS data into forest inventory attributes using an automated workflow, we used the 3DFin plugin (Laino *et al.* 2024) implemented in CloudCompare (v2.13.2). The software is openly accessible and provides all key processing steps required to derive tree attributes—height normalisation, tree detection, instance segmentation, and tree-attribute measurement—directly from TLS/MLS point cloud data. Compared with other automated workflows, it has been reported to perform well (Laino *et al.* 2024). In this study, 3DFin was applied to MLS data downsampled to a 1 mm resolution, using its default parameter settings except for adjusting the minimum stem diameter to 4 cm.

3DFin processes point-cloud data through four main stages. First, the point cloud is height-normalized using a DEM generated with the Cloth Simulation Filter. Second, a horizontal slice is extracted from the normalized point cloud, and vertical points within this slice are identified and clustered to detect stem bases. Third, initial stem axes are estimated and used to assign points to individual trees and to determine tree height. Finally, stem diameters are measured at regular vertical intervals using circle fitting, with built-in quality-control criteria applied to remove unreliable estimates. Together, these steps produce fully automatic measurements of tree attributes, which were subsequently aggregated at the plot level to derive estimates for TPH, G, V, Dg, Hg, and Hdom.

Accuracy assessment

Assessing the accuracy of detecting and characterising individual trees from MLS point clouds.

Trees detected from the MLS data were manually verified and linked to the corresponding reference trees. Manual verification was required because the reference measurements also contained random localisation errors that caused some tree positions to deviate more than expected. Additionally, up to 1.5 growing seasons had elapsed between the reference and MLS campaigns and some trees had fallen, causing some structural changes. Reference trees without a valid MLS match—typically due to incomplete reconstruction or segmentation—were labelled as ‘not segmented’ and counted as omission errors.

Tree detection accuracy was assessed separately for both workflows by computing the segmentation rate (SR) and characterisation rate (CR). SR denotes the proportion of reference trees that could be detected and segmented from the MLS data, whereas CR represents the proportion of reference trees for which tree attributes could be successfully derived. A small number of MLS-derived trees could not be matched to any reference trees, most likely due to them being missed during field data collection. These were omitted from analysis; no commission errors were therefore evaluated, as the field inventory data were treated as ground truth.

Tree characterisation accuracy was assessed for matched trees using bias and RMSE for DBH and height:

$$RMSE = \sqrt{\frac{\sum_{i=1}^{n} \left(\hat{y}_i - y_i\right)^2}{n}} \quad (1)$$

$$Bias = \frac{\sum_{i=1}^{n} \left(\hat{y}_i - y_i\right)}{n} \quad (2)$$

where y_i denotes the reference value for tree i, $\hat{y}_i$ the MLS-derived value for tree i, and n the number of trees. For height, only trees with field-measured (not model-predicted) heights were included. In addition to absolute values, we computed relative RMSE and bias by dividing by population means. Given the time lag between the reference measurements and MLS data acquisition, measurement

accuracy was expected to be affected by tree growth. To account for this possible bias, we also used Pearson's correlation coefficient (r) to evaluate the linear relationship between the field-measured and point cloud-derived measurements.

Assessing the accuracy of MLS-derived forest inventory attributes

To assess the accuracy of MLS-derived forest inventory attributes, the point-cloud-derived estimates for TPH, G, Dg, Hg, Hdom, and V were compared with those obtained from the reference data. Bias and RMSE (Equations 1–2) were used to quantify accuracy and r was used to evaluate consistency between MLS-derived and reference measurements. In Equations 1 and 2, y_i denotes the reference value for plot i, $\hat{y}_i$ the MLS-derived value for plot i, and n the number of plots.

Assessing the influence of data acquisition trajectory, processing workflow, and forest structure on the measurement accuracy

We also evaluated how data acquisition trajectory and processing workflow influenced MLS-based forest inventory performance. Performance in CR, as well as in estimating tree- and plot-level forest inventory attributes, was compared across four scenarios: the assisted workflow applied on MLS-loop (*assisted-loop*) and MLS-line data (*assisted-line*), and the automatic workflow applied on MLS-loop (automatic-loop) and MLS-line data (*automatic-line*). In addition to accuracy metrics, we analysed differences in data acquisition duration and in the total number of recorded 3D observations (stem points, crown points) for MLS-line versus MLS-loop.

To further understand the influence of forest structure on MLS-based forest inventory performance, we analysed the association between CR and forest attributes. Given that higher tree density and greater vegetation complexity are expected to affect measurement accuracy (Yrttimaa *et al.* 2019), we used r to evaluate the relationship between CR and TPH, G, Dg, Hg, Hdom, and V. In addition, we examined metrics describing tree size and variability within the sample plot, specifically the standard deviation, minimum, maximum, and mean values of DBH and tree height.

Results

Accuracy of detecting and characterizing individual trees from MLS point clouds

Using the MLS-line acquisition trajectory, 99.8% of field-measured trees were identified with the *assisted-line* approach, whereas the *automatic-line* approach identified 78.4%. For the MLS-loop trajectories, the *assisted-loop* approach detected 99.7% and *automatic-loop* detected 80.0%. After excluding trees for which DBH or height could not be derived due to incomplete point cloud reconstructions, the overall CR was 97.1% for *assisted-line* and 96.7% for *assisted-loop*. The fully automatic workflow achieved a CR of 73.7% for *automatic-line* and 74.1% for *automatic-loop*. In the assisted workflow, undetected trees were not concentrated in any particular size class, whereas the automatic workflow predominantly missed small-diameter trees (<15 cm).

For *assisted-line*, the RMSE for DBH and height were 2.4 cm (14.8%) and 2.1 m (14.0%), respectively, compared with 2.5 cm (13.3%) and 6.4 m (36.7%) for *automatic-line*. For *assisted-loop*, RMSE values were 2.7 cm (16.2%) for DBH and 2.4 m (15.7%) for height, while *automatic-loop* yielded 2.4 cm (12.5%) for DBH and 6.2 m (35.5%) for height. DBH was overestimated in all approaches, with biases of 1.4 cm for *assisted-line*, 1.5 cm for *automatic-line*, and 1.2 cm for both *assisted-loop* and *automatic-loop*. Height was underestimated by 0.2 m in both *assisted-line* and *assisted-loop*, whereas the automatic workflow overestimated height by 3.1 m for *automatic-line* and 2.8 m for *automatic-loop*.

The Pearson correlation between reference and MLS-derived DBH was 0.97 for *assisted-line*, *automatic-line*, and *automatic-loop*, and 0.96 for *assisted-loop*. For height, the correlations were 0.96 for *assisted-line* and 0.95 for *assisted-loop*, while the automatic workflow achieved correlations of 0.65 and 0.64 for *automatic-line* and *automatic-loop*, respectively. As shown in Fig. 6, the accuracy of MLS-derived DBH and height generally improved with increasing tree size, whereas the automatic workflow particularly overestimated smaller trees.

Accuracy of deriving plot-level forest inventory attributes

Strong correlations were observed between MLS-derived plot-level forest inventory attributes and reference measurements across all investigated attributes (Fig. 7). Using the assisted workflow, the correlations were ≥ 0.98 for Dg, Hg, TPH, V, and Hdom, and 0.94 for G in both *assisted-line* and *assisted-loop*. The automatic workflow also showed strong correlations for most variables, with $r \geq 0.97$ for Dg, Hg, V, and Hdom, and $r \geq 0.91$ for G. In contrast, TPH exhibited clearly weaker performance when derived using the automatic workflow, with correlations of 0.62 (*automatic-line*) and 0.66 (*automatic-loop*), indicating substantial limitations in stem detection.

The assisted workflow overestimated G, with RMSEs of 3.8 m^2/ha (bias 2.7 m^2/ha) and 3.5 m^2/ha (bias 2.2 m^2/ha) for *assisted-line* and *assisted-loop*, respectively. In contrast, the automatic workflow underestimated G: *automatic-line* yielded an RMSE of 3.6 m^2/ha and a bias of −0.5 m^2/ha, while *automatic-loop* produced an RMSE of 4.2 m^2/ha and a bias of −1.3 m^2/ha. TPH was estimated with high accuracy using the assisted workflow, with RMSEs of 51 n/ha (*assisted-line*) and 54 n/ha (*assisted-loop*) and slight negative biases (−27 n/ha and − 33 n/ha), reflecting missed trees. The automatic workflow performed substantially worse, with RMSEs exceeding 600 n/ha and biases of ∼−370 n/ha in both trajectory types, indicating major underestimation of stem density.

For Hg, *assisted-line* achieved an RMSE of 1.2 m and a bias of −0.5 m, while *assisted-loop* produced an RMSE of 1.3 m and a bias of −0.6 m. The automatic workflow yielded slightly higher RMSEs of 1.5 m (*automatic-line*) and 1.6 m (*automatic-loop*), with positive biases of 0.9 m and 0.5 m, indicating overestimation of mean height. For Dg, the assisted workflow outperformed the automatic one: a*ssisted-line* produced an RMSE of 1.0 cm (bias 0.7 cm), and *assisted-loop* an RMSE of 1.2 cm (bias 0.7 cm). In comparison, the automatic workflow showed higher errors, with RMSEs of 2.8 cm (bias 2.3 cm) for *automatic-line* and 2.3 cm (bias 1.9 cm) for *automatic-loop*, suggesting systematic overestimation of mean diameter.

V was estimated with higher precision in the assisted workflow, which yielded RMSEs of 19.1 m^3/ha (bias 11.5 m^3/ha) for *assisted-line* and 20.2 m^3/ha (bias 6.4 m^3/ha) for *assisted-loop*. In comparison, the automatic workflow resulted in higher RMSEs of 27.9 m^3/ha (bias 5.2 m^3/ha) and 29.3 m^3/ha (bias −4.8 m^3/ha), respectively. For Hdom, *assisted-line* reached an RMSE of 0.8 m (bias −0.3 m), while *assisted-loop* had an RMSE of 1.2 m (bias −0.7 m). *Automatic-line* achieved the

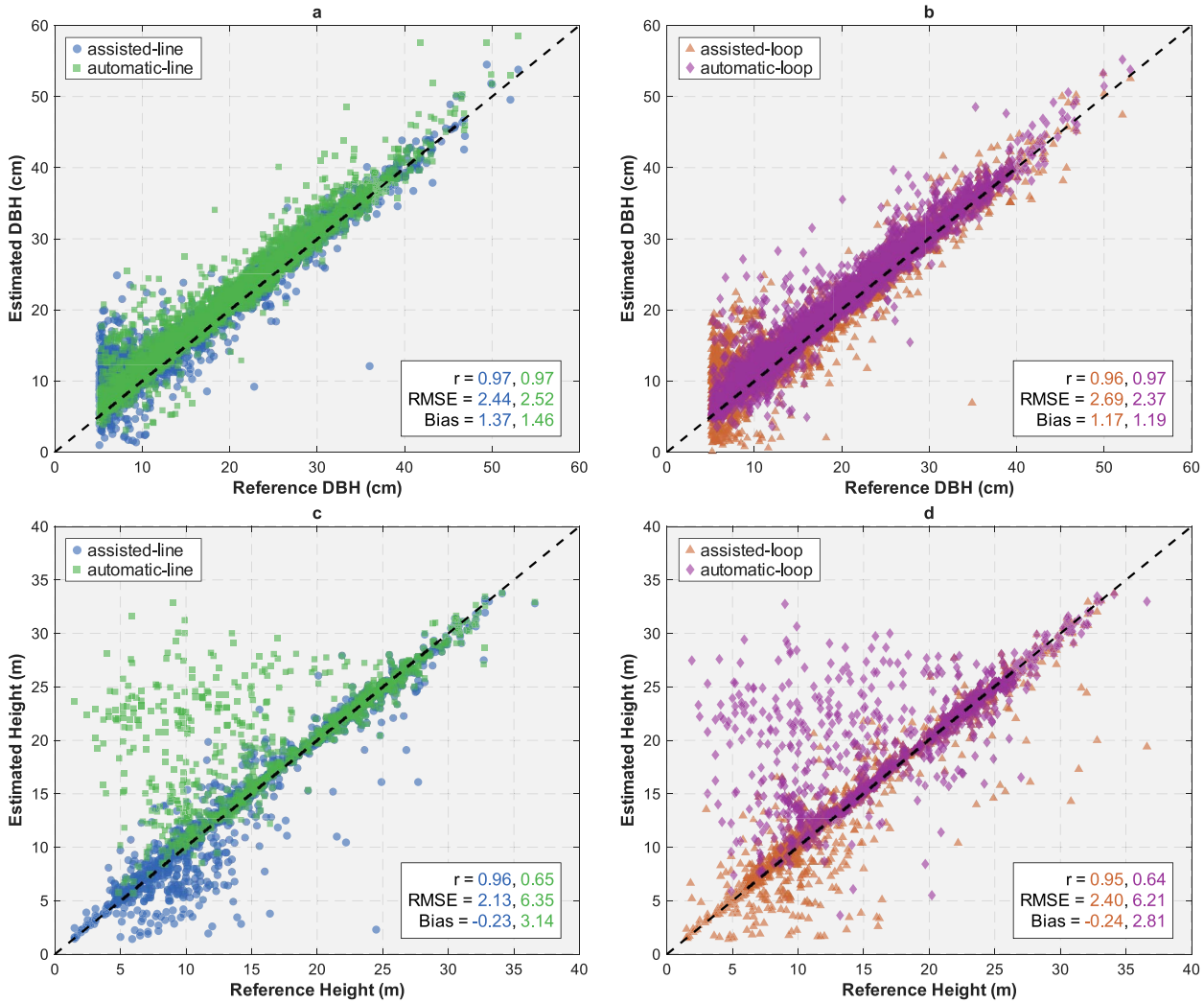

Figure 6 The relationship between measurements for DBH and height when derived during the field campaign using calipers (Reference DBH & Height) and mobile laser scanning (estimated DBH & Height). Root mean square error (RMSE), mean error (bias), and Pearson's correlation coefficient (r) are reported to facilitate comparison between the two processing approaches—*Assisted* and *automatic*—as well as the two data acquisition trajectories: Line transects (MLS-line) and closed loops (MLS-loop), as illustrated in Fig. 4.

lowest RMSE for Hdom (0.6 m) with a near-zero bias (−0.1 m), whereas *automatic-loop* performed worse (RMSE 1.9 m, bias −0.7 m).

Influence of data acquisition trajectory and forest structure on the performance of MLS-based forest inventory

Forest structure seemed to have a minor influence on the performance of the assisted workflow. Weak-to-moderate correlations (−0.33 to −0.44) were observed between CR and plot-level standard deviation of either DBH or height (Fig. 8). This suggests that a greater structural variability increased the likelihood of undetected stems, implying decreased performance in more complex stand conditions. However, because most trees were detected (SR > 99.5%) and measured (CR > 96%) using the assisted workflow, no clear association between detection performance and any specific forest variable was identified.

Using the automatic workflow, moderate to strong positive correlations (0.68–0.79) were found between CR and plot-level mean DBH and height. Other size-dependent variables such as Dg, Hg, Hdom, V, and the maximum and minimum height and DBH showed moderate correlation (0.46–0.63) with CR. Conversely, a strong negative correlation (−0.64 to −0.72) was observed between TPH and CR. Consequently, plots with larger trees and higher standing volume exhibited better detection performance. Unlike in the assisted workflow, the standard deviations of height or DBH showed no negative correlations with detection rate, further indicating that the automatic workflow systematically failed to detect part of small trees which are more abundant in plots with high TPH.

For the assisted workflow, inspection of residuals in the plot-level forest inventory attribute estimates (Fig. 7) revealed that G, Dg, and V tended to be overestimated in stands with low values of these attributes and underestimated in stands with high values. An opposite pattern was observed for Hg and Hdom. TPH was never overestimated; instead, underestimation and its variability increased as TPH increased, reflecting a higher likelihood of missed stems in denser plots.

The average data acquisition duration, including the finalisation period, was ~59.0% longer for MLS-line (30.5 min per plot on average) than for MLS-loop (19.0 min). Because the MLS device recorded data continuously, this longer data acquisition time resulted in 20.8% more

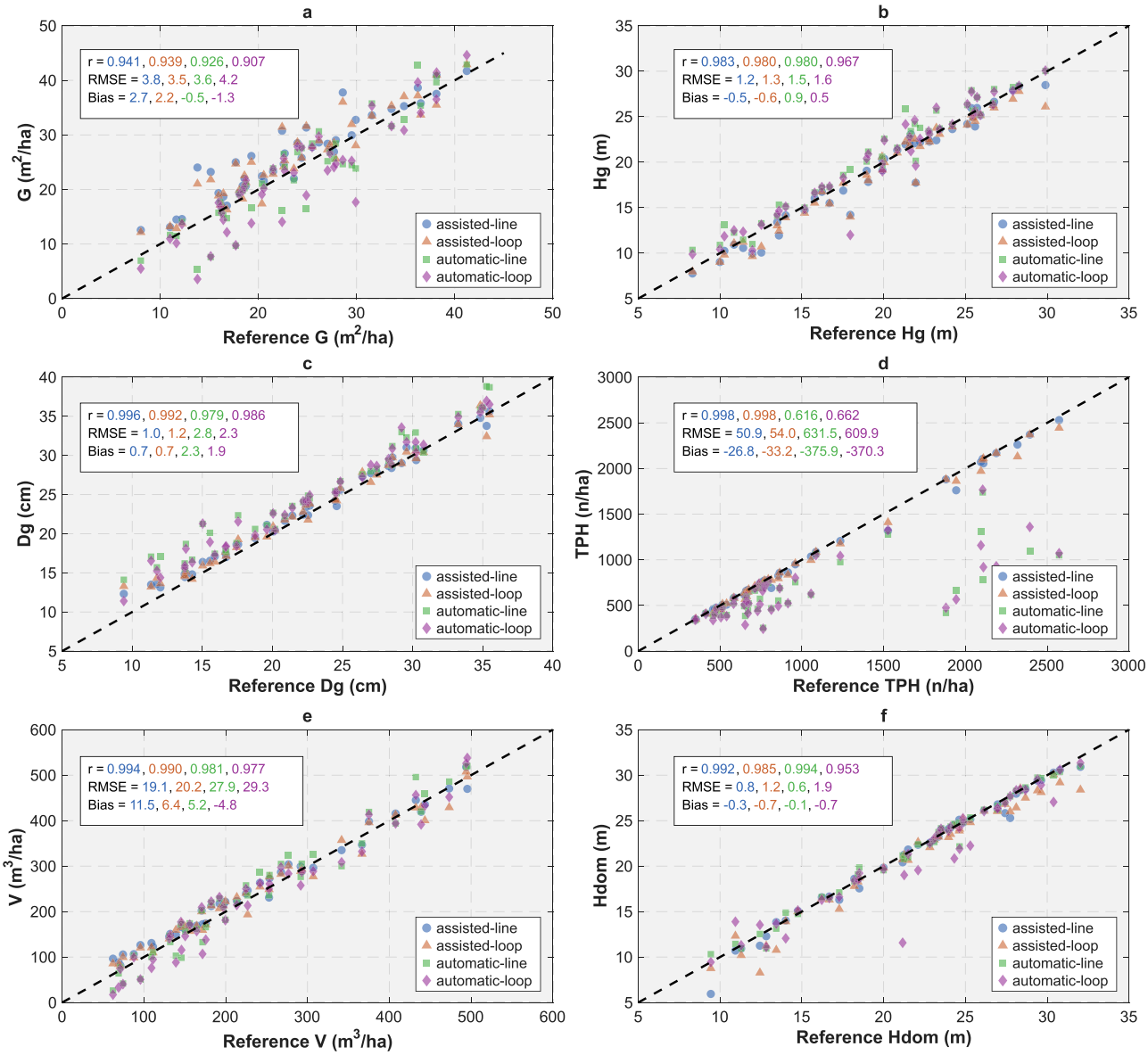

Figure 7 Relationships between estimates for plot-level forest inventory attributes when derived using the callipers, clinometers, and allometric models (reference) and mobile laser scanning (MLS). Forest inventory values include basal area (G), basal area-weighted mean tree height (Hg) and -diameter (Dg), number of trees per hectare (TPH), total stem volume (V), and dominant height (Hdom). Root mean square error (RMSE), mean error (bias), and Pearson's correlation coefficient (r) are reported to facilitate comparison between the two processing approaches—*Assisted* and *automatic*—And the two data-acquisition trajectories: Line transects (MLS-line) and closed loops (MLS-loop), as illustrated in Fig. 4.

points for MLS-line compared with MLS-loop. By semantic class, these increases corresponded to 36.2% more stem points and 16.9% more crown points. Despite the denser point cloud obtained with MLS-line, the resulting improvements in TPH, V, and Hdom estimates were marginal, and both trajectories yielded comparable accuracy for G, Hg, and Dg (Fig. 7).

Discussion

Different data acquisition trajectories

This study evaluated the feasibility of MLS for surveying boreal forest sample plots in an operational setting using two data-processing workflows: one incorporating manual assistance in tree detection and another relying on fully automatic processing. In addition, two MLS data acquisition trajectory designs were compared: a line-transect approach in which parallel trajectories crossed the sample plot at fixed intervals (MLS-line) and a closed-loop approach in which the plot was covered by four loops intersecting at the plot centre (MLS-loop). The results showed that the more intensive MLS-line approach produced more 3D observations which translated into similar or marginally improved accuracy in tree- and plot-level attribute estimates when using the assisted workflow. In contrast, under the fully automatic workflow, MLS-loop yielded more accurate tree-attribute measurements, while both trajectory designs produced similar levels of accuracy for plot level forest inventory attributes.

The findings regarding the influence of MLS trajectory design on reconstruction quality are broadly consistent with previous research. Trajectories resembling MLS-line have been shown to extend data

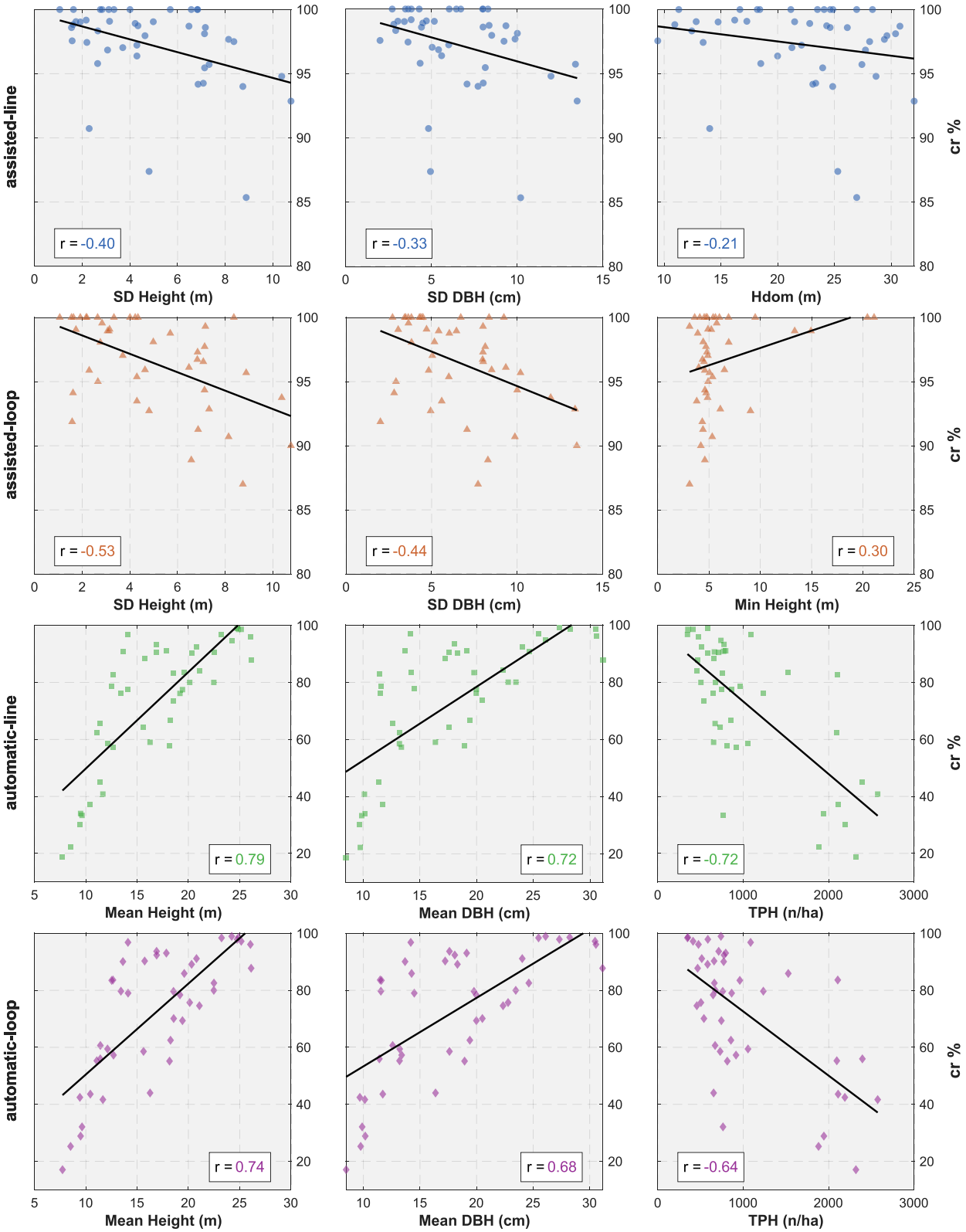

Figure 8 Relationships between forest inventory attributes and the CR (%) for different processing approaches. Three strongest Pearson's correlation coefficients (r) are shown for both *assisted* and *automatic* workflows and for the two MLS acquisition trajectories—Line transects (MLS-line) and closed loops (MLS-loop)—as illustrated in Fig. 4. The strongest correlations were observed for minimum, mean, and standard deviation (SD) of DBH and height (H), as well as for trees per hectare (TPH) and dominant height (Hdom).

acquisition duration and increase point density and data volume (Tiede *et al.* 2024), but not necessarily improve tree-attribute measurement accuracy compared with loop-based trajectories (Sofia *et al.* 2024). A likely explanation is that the increased point density also introduces additional noise, which must be accounted for during data processing. This was evident in our results: the assisted workflow, which incorporated noise mitigation during semantic segmentation, benefited from the greater data volume, whereas the automatic workflow—without noise handling tuned to MLS data—showed reduced performance under the MLS-line approach.

During our field campaign, four MLS-line data acquisitions failed during SLAM processing, whereas no failed acquisitions occurred with MLS-loop. Bauwens *et al.* (2016) reported that similar MLS data acquisition may fail in forests with either very high stem density and dense understorey or very low stem density—conditions under which SLAM tends to struggle. However, in the present study, no clear structural pattern explained the failed MLS-line acquisitions, though they may be related to the longer acquisition duration required by MLS-line. Because MLS-loop produces adequate point-cloud coverage within shorter acquisition times and does not compromise measurement accuracy relative to MLS-line, it can be considered the preferred trajectory design for operational forest inventories. Data acquisition trajectories such as our MLS-loop have also been recommended in early MLS studies (Kukko *et al.* 2017) and by sensor manufacturers. Similar data acquisition trajectories have been used in other large-scale tests (Gollob *et al.* 2020). Nevertheless, MLS trajectories should be standardized within acquisition campaigns, as variations may influence certain measurements, such as indicators of stand structural complexity (Neudam *et al.* 2022).

Individual tree characterisation for plot-level attribute estimation

Accurate detection of all relevant trees and reliable measurement of their characteristics form the basis for point cloud-based surveying of sample plots, as tree-level errors accumulate at the plot level (Yrttimaa *et al.* 2019). Missed trees cause systematic underestimation of TPH, G, and V, while systematic DBH or height errors affect Dg, Hg, and Hdom even when detection is perfect. Therefore, both detection performance and measurement accuracy must be evaluated in MLS workflows.

Automatic workflows applied to TLS and MLS data are known to struggle in detecting all relevant trees, particularly in structurally complex stands with dense understorey and numerous small trees (Liang *et al.* 2018, Yrttimaa *et al.* 2019). Across varying forest conditions, fully automatic TLS/MLS methods typically achieve detection rates of ∼70%–90% (e.g. Holvoet *et al.* 2025). Hrdina *et al.* (2025) compared several automatic tree detection and measurement algorithms in a stand of 236 trees and reported detection rates ranging from 44.5% to 97%, with DBH RMSE values of 1.6–2.4 cm. Using an assisted workflow, they achieved a detection rate of 99.2% with a DBH RMSE of 1.2 cm. The fully automatic 3DFin algorithm—also used in this study—achieved 77.1% detection with a DBH RMSE of 2.4 cm. In Austria, Gollob *et al.* (2020) achieved a detection accuracy of 96% and a DBH RMSE of 2.3 cm (12.0%) using an automatic workflow in an experimental setup comprising 2466 trees across 20 sample plots. Under operational conditions, Kükenbrink *et al.* (2025) evaluated fully automatic MLS processing across 29 Swiss NFI plots and reported an average detection accuracy of 82.6% with a DBH RMSE of 2.8 cm (7.7%).

In this study, the automatic workflow followed this pattern, detecting 73.7% of trees with a DBH RMSE of 2.5 cm and a height RMSE of 6.4 m; most missed trees had DBH < 15 cm. By contrast, the assisted workflow—which involved manual refinement of tree detection while keeping subsequent segmentation and measurement fully automated—achieved 97.1% detection with a DBH RMSE of 2.4 cm and height RMSE of 2.1 m. These results highlight the limitations of fully automated processing, while demonstrating that incorporating targeted manual assistance—particularly during tree detection—enables MLS to capture nearly all trees and produce structurally complete point-cloud reconstructions.

All results experienced low to moderate positive bias relative to the reference measurements. Part of this bias can be attributed to forest growth, as the time gap between the reference and MLS measurements ranged from 9 to 14 months, corresponding to approximately half to one and a half growing seasons. Particularly in young forests, this can result in centimetre-level DBH increments, and height increases of several decimetres (e.g. Männistö *et al.* 2024). In addition, a portion of the positive DBH bias is likely related to noise caused by laser-beam divergence. Unlike random noise, beam divergence increases the laser footprint with distance, producing edge returns that systematically inflate the fitted stem diameters (Faitli *et al.* 2024). For tree height—derived from the highest point return associated with each tree—the largest errors were primarily caused by inaccuracies in instance segmentation, a problem that was more pronounced in the automatic workflow. In multilayered stands, points from lower canopy layers were often misassigned to upper canopies, leading to systematic overestimation of tree height. This effect was reflected in the observed positive height biases of 2.1 m for the *assisted-line* and 6.4 m for the *automatic-line* workflows.

For operational forest inventories, the primary objective is the accurate estimation of plot-level attributes; however, evaluations of MLS- or TLS-based performance at the plot level remain relatively scarce. Vatandaşlar *et al.* (2023) assessed MLS-derived forest inventory attributes across 39 plots and reported RMSEs of 8.4% for TPH, 10.1% for G, 4.5% for Dg, 9.4% for Hdom, and 16.4% for V. Similar to our assisted workflow, their approach combined automatic stem detection with a visual inspection step to correct tree locations when necessary. Using TLS data and fully automatic processing in comparable boreal forest conditions, Yrttimaa *et al.* (2019) reported correlations of 0.82–0.97 between TLS-derived and field-measured attributes and RMSEs of 12.3% for Dg, 5.9% for Hg, 18.4% for G, 51.7% for TPH, and 15.3% for V. In the present study, the assisted workflow achieved strong correlations with the reference data ($r > 0.94$) and low relative RMSEs (< 8%) for TPH, Hg, Dg, V, and Hdom, while G showed a higher RMSE of 16.3%. In contrast, the fully automatic 3DFin workflow exhibited substantially higher errors, with an RMSE of 61.9% for TPH and 12–15% for most other attributes, except for Hdom (2.9%).

Overall, these results highlight the importance of applying assisted workflows for attributes sensitive to detection completeness, particularly TPH. For other attributes (Dg, Hg, Hdom, G, V), differences between workflows were smaller. The comparison further demonstrates that kinematic MLS acquisition enables efficient capture of the complete forest scenes while maintaining plot-level measurement accuracy comparable to static TLS, despite the higher noise levels inherent in MLS point cloud data.

Operational feasibility and future perspectives

While the experiments conducted in this study demonstrate that MLS has strong potential as a feasible technology for forest surveying, further development of post-processing solutions and standardized

protocols is required. Accurate instance segmentation remains a major bottleneck, as it determines the population of successfully characterized trees and the reliability of their derived attributes. To address known challenges of detecting all trees in structurally complex forests (e.g. Liang *et al.* 2018, Calders *et al.* 2020), we applied an assisted workflow and compared its performance with fully automatic measurements generated using 3DFin. The assisted workflow, relying on manual tree detection confirmation followed by automated subsequent processing, consistently produced more accurate plot-level forest inventory attribute estimates. These results indicate that future improvements should primarily target the most uncertain processing step—instance segmentation. Encouragingly, recent advances in sensor-agnostic point-cloud segmentation methods, including machine- and deep-learning-based approaches (e.g. Wielgosz *et al.* 2024), are likely to substantially alleviate this limitation in the near future.

The operationally more feasible automatic workflow proved reliable in plots with relatively simple stand structures, whereas layered canopies and high densities of small-diameter trees led to missed detections and segmentation errors. This is particularly relevant in our study area, where 30% of the trees had a DBH below 10 cm and 50% were below 15 cm. These shortcomings resulted in substantial underestimation of TPH and affected height estimation. In contrast, plot-level variables such as Hdom, Hg, and Dg remained accurate, as they are less sensitive to omissions of small trees.

An important aspect not addressed in this study—but crucial for operational deployment—is the occurrence and impact of false positives (commission errors) in automatic tree detection. Such errors may arise from seedlings below the diameter threshold or from branches misclassified as stems. In the assisted workflow, these errors were manually removed, whereas in the automatic workflow no correction was applied, potentially introducing additional bias. Developing robust methods for automatical identification and removal of false detections, and systematically assessing their impact, should therefore be investigated in future research.

From an operational perspective, MLS has been shown to substantially reduce both field and office workload, thereby lowering the overall costs of surveying sample plots (Sofia *et al.* 2024). Hunčaga *et al.* (2020) reported MLS data acquisition to be ~5.3 times faster than TLS, while Gollob *et al.* (2020) found MLS to be 2.5 times faster than traditional field measurements. Shifting effort from field work to office-based point cloud analysis allows more comprehensive data capture and analysis while maintaining overall efficiency. Even with assisted processing, MLS-based workflows can be operationally feasible when supported by streamlined software solutions. The increasing availability of open-source tools (Laino *et al.* 2024) and more affordable MLS devices has further lowered adoption barriers (Balestra *et al.* 2024).

Although software capable of fully automatic extraction of individual-tree attributes already exists, there remains substantial scope for further automation. In particular, user-friendly tools that integrate the entire workflow—from raw data processing to tree- and plot-level attribute computation—are essential to enable wider operational adoption. In line with recent studies (e.g. Pires *et al.* 2024), our results demonstrate that current MLS technology is already a viable and promising alternative for forest sample-plot measurements, provided that remaining post-processing challenges are addressed. Finally, forest inventory attributes are typically derived by tree species, which was not considered in this study. While tree species recognition using geometric data alone is feasible (Åkerblom *et al.* 2017), incorporating spectral information—such as data from imagery or multispectral laser scanning—could further improve classification accuracy (Chen *et al.* 2024) and enable the estimation of species-specific forest inventory attributes.

Conclusion

The experiments conducted in this study across a range of boreal forest conditions demonstrate that MLS is a suitable technology for rapidly collecting point cloud data for accurate forest surveying. Potential use cases include sample-plot measurements for NFIs, ALS-based forest inventories, forest research, and quality control of forest operations. Most forest inventory attributes—except TPH—were measured reliably using automatic workflows. However, incorporating manual assistance during tree detection revealed the full potential of MLS, acknowledging that tree detection and instance segmentation currently represent the main computational bottlenecks in point-cloud-based forest characterisation. These limitations are expected to diminish as computational methods continue to improve.

Comparisons between alternative data acquisition trajectories showed that the more intensive MLS-line approach generally produced higher point density and reduced occlusion. In the assisted workflow, this translated into slightly improved individual-tree measurement accuracy. In contrast, under fully automatic processing, MLS-loop yielded more accurate results. Increased point density did not consistently improve plot-level forest inventory attribute estimates. The repeated loop closures inherent in MLS-loop appeared to benefit SLAM performance, as no acquisition failures were observed. Nevertheless, intensifying data acquisition may still be advantageous in some situations; therefore, increasing the number of loops (or 'petals') within the MLS-loop design may help ensure sufficient data capture in large sample plots or structurally complex forest stands.

Declaration of Generative AI and AI-assisted technologies in the writing process

During the preparation of this work, the authors used ChatGPT-5 to check grammar and improve the clarity of the text. After using this tool, the authors reviewed and edited the content as needed, taking full responsibility for the final publication.

Acknowledgements

In addition, the authors wish to acknowledge CSC—IT Center for Science, Finland, for computational resources. The authors also acknowledge the collaboration and support related e.g. to fieldwork and study design provided through the project KESSU—Improving the Availability of Sustainably Produced Small-Diameter Wood in North Karelia ('Kestävästi tuotetun pienpuun saatavuuden parantaminen Pohjois-Karjalassa'). The preparation of this research article was not funded by the KESSU. The KESSU project is funded by the Regional Council of North Karelia ('Pohjois-Karjalan Maakuntaliitto') and co-financed by the European Union.

Author contributions

Lauri Liikonen (Formal analysis, Investigation, Methodology, Validation, Visualization, Writing—original draft), Tuomas Yrttimaa (Conceptualization, Software, Supervision, Writing—original draft),

Aapo Erkkilä (Data curation, Investigation, Writing—review & editing), Johanna Paakkari (Investigation, Writing—review & editing), Eetu Kotivuori (Conceptualization, Investigation, Resources, Writing—review & editing), Timo P Pitkänen (Conceptualization, Investigation, Writing—review & editing), and Mikko Vastaranta (Conceptualization, Funding acquisition, Resources, Writing—review & editing)

Conflict of interest

None declared.

Funding

This study was supported by the Research Council of Finland through funding provided for the UNITE flagship [grant number 357906], Scan4est Research Infrastructure [grant number 346383], Diversity4Forests project [grant number 348643] and MULTIRISK project [grant number 353262]. It should be noted that the funding for the Diversity4Forests project originates from the European Union's NextGenerationEU initiative. Views and opinions expressed are, however, those of the authors only and do not necessarily reflect those of the European Union or the European Research Council Executive Agency. Neither the European Union nor the granting authority can be held responsible for them.

Data availability

The data that support the findings of this study are available from the corresponding author upon reasonable request.

References

Åkerblom M, Raumonen P, Mäkipää R. *et al.* Automatic tree species recognition with quantitative structure models. *Remote Sens Environ* 2017;**191**:1–12. https://doi.org/10.1016/j.rse.2016.12.002

Aschoff T, Spiecker H. Algorithms for the automatic detection of trees in laser scanner data. Int. *Arch Photogramm Remote Sens Spat Inf Sci* 2004;**36**:66–70.

Axelsson P. DEM generation from laser scanner data using adaptive TIN models. *Int Arch Photogramm Remote Sens* 2000;**33**:110–7.

Balenović I, Liang X, Jurjević L. *et al.* Hand-held personal laser scanning – current status and perspectives for forest inventory application. *Croat J For Eng* 2021;**42**:165–83. https://doi.org/10.5552/crojfe.2021.858

Balestra M, Cabo C, Murtiyoso A. *et al.* Advancing forest inventory: a comparative study of low-cost MLS lidar device with professional laser scanners. *Int Arch Photogramm Remote Sens Spatial Inf Sci* 2024;**XLVIII-2/W8-2024**:9–15. https://doi.org/10.5194/isprs-archives-XLVIII-2-W8-2024-9-2024

Bauwens S, Bartholomeus H, Calders K. *et al.* Forest inventory with terrestrial LiDAR: a comparison of static and hand-held mobile laser scanning. *Forests* 2016;**7**:127. https://doi.org/10.3390/f7060127

Bremer M, Wichmann V, Rutzinger M. Multi-temporal fine-scale modelling of Larix decidua forest plots using terrestrial LiDAR and hemispherical photographs. *Remote Sens Environ* 2018;**206**:189–204. https://doi.org/10.1016/j.rse.2017.12.023

Calders K, Adams J, Armston J. *et al.* Terrestrial laser scanning in forest ecology: expanding the horizon. *Remote Sens Environ* 2020;**251**:112102. https://doi.org/10.1016/j.rse.2020.112102

Chen J, Liang X, Liu Z. *et al.* Tree species recognition from close-range sensing: a review. *Remote Sens Environ* 2024;**313**:114337. https://doi.org/10.1016/j.rse.2024.114337

Chisholm RA, Cui J, Lum SKY. *et al.* UAV LiDAR for below-canopy forest surveys. *J Unmanned Veh Syst* 2013;**1**:61–68. https://doi.org/10.1139/juvs-2013-0017

Dassot M, Constant T, Fournier M. The use of terrestrial LiDAR technology in forest science: application fields, benefits and challenges. *Ann For Sci* 2011;**68**:959–74. https://doi.org/10.1007/s13595-011-0102-2

Di Stefano F, Chiappini S, Gorreja A. *et al.* Mobile 3D scan LiDAR: A literature review. *Geomatics Nat Hazards Risk* 2021;**12**:2387–429. https://doi.org/10.1080/19475705.2021.1964617

Eerikäinen K. A multivariate linear mixed-effects model for the generalization of sample tree heights and crown ratios in the Finnish national forest inventory. *For Sci* 2009;**55**:480–93. https://doi.org/10.1093/forestscience/55.6.480

Ester M, Kriegel H-P, Sander J. *et al.* A density-based algorithm for discovering clusters in large spatial databases with noise. In: *Proc. 2nd Int. Conf. Knowl. Discov. Data Min. (KDD'96), Portland, Oregon*, 1996, 226–31.

Faitli T, Hyyppä E, Hyyti H. *et al.* Integration of a mobile laser scanning system with a forest harvester for accurate localization and tree stem measurements. *Remote Sens* 2024;**16**:3292. https://doi.org/10.3390/rs16173292

FARO Technologies Inc. *Orbis™ Mobile Scanner and Datalogger User Manual*. Lake Mary, FL: FARO Technologies Inc., 2024. https://download.faro.com/ui/core/index.html?mode=public&referrer=%2Furl%2Fbvzxaum2riwmmjws#expl-tabl./SHARED/!1zs4FG8kQgxjO/cbPwENF3KPJQmlvR Accessed 11 Mar. 2025.

Fischler MA, Bolles RC. Random sample consensus: a paradigm for model fitting with applications to image analysis and automated cartography. *Commun ACM* 1981;**24**:381–95. https://doi.org/10.1145/358669.358692

Gobakken T, Næsset E. Assessing effects of positioning errors and sample plot size on biophysical stand properties derived from airborne laser scanner data. *Can J For Res* 2009;**39**:1036–52. https://doi.org/10.1139/X09-025

Gollob C, Ritter T, Nothdurft A. Forest inventory with long range and high-speed personal laser scanning (PLS) and simultaneous localization and mapping (SLAM) technology. *Remote Sens* 2020;**12**:1509. https://doi.org/10.3390/rs12091509

Groiss B, Handl M. Efficient extraction of tree parameters from 3D point clouds. Oral presentation at: EGU Gen. Assem. 2024, Vienna, Austria, 14–19 Apr 2024. EGU24-9834. 2024. https://doi.org/10.5194/egusphere-egu24-9834

Henning JG, Radtke PJ. Ground-based laser imaging for assessing three-dimensional forest canopy structure. *Photogramm Eng Remote Sensing* 2006;**72**:1349–58. https://doi.org/10.14358/PERS.72.12.1349

Holvoet J, Eichhorn MP, Giannetti F. *et al.* Terrestrial and mobile laser scanning for national forest inventories: from theory to implementation. *Remote Sens Environ* 2025;**329**:114947. https://doi.org/10.1016/j.rse.2025.114947

Hrdina M, Molina-Valero JA, Kuželka K. *et al.* Obtaining the highest quality from a low-cost Mobile scanner: a comparison of several pipelines with a new scanning device. *Remote Sens* 2025;**17**:2564. https://doi.org/10.3390/rs17152564

Hunčaga M, Chudá J, Tomaštík J. *et al.* The comparison of stem curve accuracy determined from point clouds acquired by different terrestrial remote sensing methods. *Remote Sens* 2020;**12**:2739. https://doi.org/10.3390/rs12172739

Hyyppä E, Yu X, Kaartinen H. *et al.* Comparison of backpack, handheld, under-canopy UAV, and above-canopy UAV laser scanning for field reference data collection in boreal forests. *Remote Sens* 2020;**12**:3327. https://doi.org/10.3390/rs12203327

Iglhaut J, Cabo C, Puliti S. *et al.* Structure from motion photogrammetry in forestry: a review. *Curr For Rep* 2019;**5**:155–68. https://doi.org/10.1007/s40725-019-00094-3

Illingworth J, Kittler J. The adaptive Hough transform. *IEEE Trans Pattern Anal Mach Intell* 1987;**PAMI-9**:690–8. https://doi.org/10.1109/TPAMI.1987.4767964

Jaakkola A, Hyyppä J, Kukko A. *et al.* A low-cost multi-sensoral mobile mapping system and its feasibility for tree measurements. *ISPRS J. Photogramm. Remote Sens.* 2010;**65**:514–22. https://doi.org/10.1016/j.isprsjprs.2010.08.002

Kostensalo J, Mehtätalo L, Tuominen S. *et al.* Recreating structurally realistic tree maps with airborne laser scanning and ground measurements. *Remote Sens Environ* 2023;**298**:113782. https://doi.org/10.1016/j.rse.2023.113782

Kükenbrink D, Marty M, Rehush N. *et al.* Evaluating the potential of handheld mobile laser scanning for an operational inclusion in a national forest inventory – a Swiss case study. *Remote Sens Environ* 2025;**321**:114685. https://doi.org/10.1016/j.rse.2025.114685

Kukko A, Kaijaluoto R, Kaartinen H. *et al.* Graph SLAM correction for single scanner MLS forest data under boreal forest canopy. *ISPRS J Photogramm Remote Sens* 2017;**132**:199–209. https://doi.org/10.1016/j.isprsjprs.2017.09.006

Laasasenaho J. Taper curve and volume functions for pine, spruce and birch. *Commun Inst For Fenn* 1982;**108**:74.

Laino D, Cabo C, Prendes C. *et al.* 3DFin: a software for automated 3D forest inventories from terrestrial point clouds. *For. Int. J. For. Res.* 2024;**97**:479–96. https://doi.org/10.1093/forestry/cpae020

Liang X, Hyyppä J, Kaartinen H. *et al.* International benchmarking of terrestrial laser scanning approaches for forest inventories. *ISPRS J. Photogramm. Remote Sens.* 2018;**144**:137–79. https://doi.org/10.1016/j.isprsjprs.2018.06.021

Liang X, Hyyppä J, Kukko A. *et al.* The use of a mobile laser scanning system for mapping large forest plots. *IEEE Geosci Remote Sens Lett* 2014b;**11**:1504–8. https://doi.org/10.1109/LGRS.2013.2297418

Liang X, Kankare V, Hyyppä J. *et al.* Terrestrial laser scanning in forest inventories. *ISPRS J Photogramm Remote Sens* 2016;**115**:63–77. https://doi.org/10.1016/j.isprsjprs.2016.01.006

Liang X, Kankare V, Yu X. *et al.* Automated stem curve measurement using terrestrial laser scanning. *IEEE Trans Geosci Remote Sens* 2014a;**52**:1739–48. https://doi.org/10.1109/TGRS.2013.2253783

Liang X, Kukko A, Balenović I. *et al.* Close-range remote sensing of forests: the state of the art, challenges, and opportunities for systems and data acquisitions. *IEEE Geosci Remote Sens Mag* 2022;**10**:32–71. https://doi.org/10.1109/MGRS.2022.3168135

Liu Z, Kaartinen H, Hakala T. *et al.* Ultra-wideband-based method for measuring tree positions with decimeter-level accuracy under a forest canopy. *IEEE J Sel Top Appl Earth Obs Remote Sens* 2025;**18**:12961–72. https://doi.org/10.1109/JSTARS.2025.3569958

Maltamo M, Næsset E, Vauhkonen J. *Forestry Applications of Airborne Laser Scanning*. Concepts and case studies. Manag. For. Ecosyst. 27. Dordrecht: Springer, 2014, 460. https://doi.org/10.1007/978-94-017-8663-8

Maltamo M, Packalen P, Kangas A. From comprehensive field inventories to remotely sensed wall-to-wall stand attribute data—a brief history of management inventories in the Nordic countries. *Can J For Res* 2021;**51**:257–66. https://doi.org/10.1139/cjfr-2020-0322

Männistö L, Miina J, Huuskonen S. How to utilize natural regeneration of birch to establish mixed spruce-birch forests in Finland? *Silva Fenn* 2024;**58**:23075. https://doi.org/10.14214/sf.23075

Morsdorf F, Kükenbrink D, Schneider FD. *et al.* Close-range laser scanning in forests: towards physically based semantics across scales. *Interface Focus* 2018;**8**:20170046. https://doi.org/10.1098/rsfs.2017.0046

Murtiyoso A, Cabo C, Singh A. *et al.* A review of software solutions to process ground-based point clouds in forest applications. *Curr For Rep* 2024;**10**:401–19. https://doi.org/10.1007/s40725-024-00228-2

Neudam L, Annighöfer P, Seidel D. Exploring the potential of mobile laser scanning to quantify forest structural complexity. *Front Remote Sens* 2022;**3**:861337. https://doi.org/10.3389/frsen.2022.861337

Olofsson K, Holmgren J. Single tree stem profile detection using terrestrial laser scanner data, flatness saliency features and curvature properties. *Forests* 2016;**7**:207. https://doi.org/10.3390/f7090207

Pires RP, Lindberg E, Persson HJ. *et al.* Mobile laser scanning as reference for estimation of stem attributes from airborne laser scanning. *Remote Sens Environ* 2024;**315**:114414. https://doi.org/10.1016/j.rse.2024.114414

Puliti S, Lines ER, Müllerová J. *et al.* Benchmarking tree species classification from proximally sensed laser scanning data: introducing the FOR-species20K dataset. *Methods Ecol Evol* 2025;**16**:801–18. https://doi.org/10.1111/2041-210X.14503

Russell MB, Fraver S, Aakala T. *et al.* Quantifying carbon stores and decomposition in dead wood: a review. *For Ecol Manage* 2015;**350**:107–28. https://doi.org/10.1016/j.foreco.2015.04.033

Simonse M, Aschoff T, Spiecker H. *et al.* Automatic determination of forest inventory parameters using terrestrial laser scanning. In: *Proc. of the ScandLaser scientific workshop on airborne laser scanning of forests 2003. Sveriges Lantbruksuniversitet, Umeå*, 2003, 252–8.

Sofia S, Giannetti F, Buscarini S. *et al.* Comparing efficiency, timing and costs of different walking paths in HMLS LiDAR survey. *Ann For Res* 2024;**67**:87–107. https://doi.org/10.15287/afr.2024.3671

Tiede J, Reinke K, Jones S. Evaluating the efficacy of sampling acquisition paths for mapping vegetation structure using terrestrial mobile laser scanning. *Ecol Inform* 2024;**82**:102675. https://doi.org/10.1016/j.ecoinf.2024.102675

Tomppo E, Olsson H, Ståhl G. *et al.* Combining national forest inventory field plots and remote sensing data for forest databases. *Remote Sens Environ* 2008;**112**:1982–99. https://doi.org/10.1016/j.rse.2007.03.032

Vatandaşlar C, Seki M, Zeybek M. Assessing the potential of mobile laser scanning for stand-level forest inventories in near-natural forests. *For Int J For Res* 2023;**96**:448–64. https://doi.org/10.1093/forestry/cpad016

Verhelst TE, Calders K, Burt A. *et al.* Implications of pulse frequency in terrestrial laser scanning on forest point cloud quality and individual tree structural metrics. *Remote Sens* 2024;**16**:4560. https://doi.org/10.3390/rs16234560

Westoby MJ, Brasington J, Glasser NF. *et al.* 'Structure-from-motion' photogrammetry: a low-cost, effective tool for geoscience applications. *Geomorphology* 2012;**179**:300–14. https://doi.org/10.1016/j.geomorph.2012.08.021

White JC, Tompalski P, Bater C. *et al.* Enhanced forest inventories in Canada: implementation, status, and research needs. *Can J For Res* 2025;**55**:1–37. https://doi.org/10.1139/cjfr-2024-0255

Wielgosz M, Puliti S, Xiang B. *et al.* SegmentAnyTree: a sensor and platform agnostic deep learning model for tree segmentation using laser scanning data. *Remote Sens Environ* 2024;**313**:114367. https://doi.org/10.1016/j.rse.2024.114367

Wilkes P, Lau A, Disney M. *et al.* Data acquisition considerations for terrestrial laser scanning of forest plots. *Remote Sens Environ* 2017;**196**:140–53. https://doi.org/10.1016/j.rse.2017.04.030

Wu Y, Zhong S, Ma Y. *et al.* Application of SLAM-based mobile laser scanning in forest inventory: methods, progress, challenges, and perspectives. *Forests* 2025;**16**:920. https://doi.org/10.3390/f16060920

Yrttimaa T. Automatic point cloud processing tools to characterize trees (point-cloud-tools: v1.0.1). *Zenodo.* 2021. https://doi.org/10.5281/zenodo.5779288

Yrttimaa T, Kankare V, Luoma V. *et al.* A method for identifying and segmenting branches of Scots pine (Pinus sylvestris L.) trees using terrestrial laser scanning. *For Int J For Res* 2024;**97**:531–45. https://doi.org/10.1093/forestry/cpad062

Yrttimaa T, Liikonen L, Erkkilä A. *et al.* Terrestrial laser scanning point clouds and tree attributes from 55 sample plots at the evo test site (spring 2024). *Silva Fenn* 2025;**59**:24066. https://doi.org/10.14214/sf.24066

Yrttimaa T, Saarinen N, Kankare V. *et al.* Investigating the feasibility of multi-scan terrestrial laser scanning to characterize tree communities in southern boreal forests. *Remote Sens* 2019;**11**:1423. https://doi.org/10.3390/rs11121423

Yrttimaa T, Saarinen N, Kankare V. *et al.* Performance of terrestrial laser scanning to characterize managed Scots pine (Pinus sylvestris L.) stands is dependent on forest structural variation. *ISPRS J. Photogramm. Remote Sens.* 2020;**168**:277–87. https://doi.org/10.1016/j.isprsjprs.2020.08.017

Forestry: An International Journal of Forest Research, 2026, **99**, cpag028
https://doi.org/10.1093/forestry/cpag028
Original Article